Università degli Studi di Genova

Scuola di Scienze Mediche e Farmaceutiche

DINOGMI

Imaging biomarkers as outcome measures for hereditary and acquired neuromuscular diseases

Candidate

Federico ZAOTTINI

Tutors

Prof. Angelo SCHENONE

Prof. Carlo MARTINOLI

Table of contents

Recently published:

Pistoia F, Picasso R, Zaottini F, Sanguinetti S, Caprioli S, Tovt L, Pansecchi M, Martinoli C. High-Resolution Ultrasound of Facial Muscles: Sonoanatomy, Scanning Technique, and Pathological Cases. J Ultrasound Med. 2023 Feb;42(3):547-557. doi:10.1002/jum.16036.

Möller Parera I, Miguel M, Blasi J, Piccaso R, Hammer HB, Ortiz-Sagrista J, Zaottini F, Martinoli C, Terslev L. Ultrasound assessment of degenerative muscle sarcopenia: the University of Barcelona ultrasound scoring system for sarcopenia. RMD Open. 2023 Jan;9(1):e002779. doi: 10.1136/rmdopen-2022-002779.

The generic term *biomarkers* applies to all detection methods used in the life sciences and may be defined as any detectable biologic parameter, whether biochemical, genetic, histologic, anatomic, physical, functional, or metabolic. By logical extension, we define imaging biomarkers as any anatomic, physiologic, biochemical, or molecular parameter detectable with one or more diagnostic imaging tools for establishing the presence and/or severity of disease.
The importance of medical imaging for clinical decision making has been steadily increasing over the last four decades. Recently, there has also been an emphasis on medical imaging for preclinical decision making, i.e., for use in pharamaceutical and medical device development. There is also a drive towards quantification of imaging findings by using quantitative imaging biomarkers, which can improve sensitivity, specificity, accuracy and reproducibility of imaged characteristics used for diagnostic and therapeutic decisions. During the three-years Phd project, in collaboration with the Radiology Department of Polililclinico San Martino/ Dipartimento di Scienze della Salute, the Neurology Unit of Policlinico San Martino / Dipartimento di Scienza della Salute and the Anatomy Departement of University of Barcelona/Campus Bellvitge, the clinical applications of new or recently developed imaging biomarkers based on High Resolution Ultrasound (HRUS) a Magnetic Resonance (MR) in the field of neuromuscular diseases have been indagated. Different clinical and one preclinical studies have been carried out to elucidate the role of HRUS and MRI imaging in the diagnosis and follow-up of hereditary and acquired neuropathies and myopathies. Regarding the conditions affecting muscle, a specific focus was sarcopenia and the Ultrasound-derived quantitative or semiquantitative parameters to identify this common condition and to help in the patient monitoring. One clinical and one Preclinical studies were funded with grants from the Italian Ministery of Health. In the following paragraphs, the different studies are presented.

NERVE DISORDERS

High Frequency Ultrasound fascicular mapping of posterior interosseous nerve

in collaboration with Professor Maribel Miguel Pérez, Unidad de Anatomía y Embriología Humana, Departamento de Patología y Terapéutica Experimental, Universidad de Barcelona

---

The somatotopic organization of the CNS has been investigated in detail but little is known about the internal topography of peripheral nerves. The classic works by Sunderland (1) posited the idea of widespread “plexiform” intermingling of fascicles within a given nerve. These results questioned the concept of an interindividual consistent somatotopy, that is, a reproducible topographic organization of fascicles within peripheral nerves. Subsequent studies, however, collected evidence for a high degree of spatial preservation of nerve fascicles positioning in cross-section[2]. These mainly experimental reports investigated the more accessible, distal portions of peripheral nerves ex vivo and found a consistent somatotopic ordering of fascicles in a “cable-like” fashion, which corresponded to the spatial-anatomical arrangement of supplied target muscles and skin

areas (1) Detection of partial and somatotopically ordered lesions in peripheral nerves can be of significant diagnostic value as was recently shown by visualization of proximal median nerve lesions isolated to motor fascicles in anterior interosseous neuropathy (2,3). In this series, we report in vivo findings from High Resolution Ultrasound demonstrating by fascicular lesion topography the somatotopy of the posterior interosseous nerve.

At the elbow level, proximal to the supinator muscle, the radial nerve splits into a sensory and a motor branch, this latter referred to as the posterior interosseous nerve (PIN). Soon after its origin, the PIN deepens and engages into the supinator tunnel, which consists of a tight passage between the superficial (SSH) and the deep (SDH) heads of the supinator muscle. Impingement of this nerve at the level of the supinator tunnel may result in the so-called PIN syndrome, a rare condition characterized by disfunction of the extensor muscles of the forearm with inability of extending the wrist and the fingers.
Occupations with repetitive prono-supination movements were considered a risk factor for PIN although, owing to the relative infrequency of this condition, no data exist to confirm the magnitude of this risk.
From its origin to its distal divisions, the PIN passes beneath several potential compressing points, including the arcade of Frohse, the sharp medial border of the extensor carpi radialis brevis, the radial recurrent blood vessels (i.e. the leash of Henry) and the inferior edge of the superficial layer of the supinator muscle (4,6).Amongst them, the arcade of Frohse is mentioned as the most frequent site of PIN entrapment. This structure is nothing more than the proximal aponeurotic part of the SSH and, in approximately 80% of people, consists of a tight tendinous arch under which the PIN travels as it engages the supinator tunnel (7). However, several more compression points may be found along the nerve path inside the supinator. Fibrous bands and, less commonly, space-occupying masses may entrap the PIN inside the tunnel. Moreover, as the supinator itself acts as a fixation point for the nerve, the PIN may also be damaged in the context of proximal stretching injuries of the radial nerve, as in the case of humeral shaft fractures (8). However, scanty literature and no imaging papers have been yet published describing the different patterns of PIN injuries distal to the Arcade of Frhose (9,10) where the PIN in divided in many fascicle, eachone with a specific muscular target. It's also unclear the prevalence of such a distal compression in patients affected by posterior interosseous neuropathy. On the other hand, identification of the level of nerve damage is critical, as an unrecognized distal compression may be a cause of failure of surgical release.
Based on these considerations, the second purpose of this study is to determine the value of high-resolution ultrasound (US) to detect the entrapment of the PIN underneath the distal edge of the supinator tunnel,

Anatomical Considerations

At the distal margin of the supinator tunnel, the basic pattern of division of the PIN is very variable among people and, not uncommonly, between the right and left side of the same person[9]. In its most typical configuration, the PIN leaves the supinator tunnel forming a wide common leash that gives off six divisional branches(11,12). The two most ulnar branches (#1,#2) are short and supply the extensor digitorum communis (EDC). One of them (#1) has a recurrent course curving upward to supply the proximal part of this muscle. Due to its superficial location, this branch is predisposed to incidental injury during surgical procedures for PIN decompression, such as the Thompson's approach. Its selective injury is associated with the "sign of horns", which refers to the inability of extending the middle and ring fingers with concomitant unaffected extension of

the index and little fingers. This sign results from an isolated loss of function of the EDC with preserved function of the extensor indicis proprius (EIP) and the extensor digiti minimi (EDM), that are supplied by other PIN divisions. Close to the EDC branches, some tiny filaments for the ECU (#3) and the EDM (#4) can be recognized. From the radial side of the leash, two major long branches descend the mid-proximal forearm as paired bundles with vertical course, the medial (#5) to provide motor supply to the EPL and the EIP, the lateral (#6) to the extensor pollicis longus (EPL), the extensor pollicis brevis (EPB) and the dorsal wrist capsule respectively. These latter nerves travelled over the deep layer of muscles of the dorsal compartment or may have a deeper course along the interosseous membrane (11,12). Lastly, an accessory recurrent branch for the supinator muscle may arise from the most radial aspect of the leash.

Materials and Methods

PIN Localization and Injection Technique in a Cadaveric Model

A cadaveric study was performed on n=3 fresh frozen elbow specimens to verify the correspondence between the anatomical and US localization of the PIN as the nerve emerges from the supinator tunnel and splits into its terminal branches. The specimens were thawed at room temperature immediately prior to the study and evaluated with US before starting the dissection. Prior to dissection, two musculoskeletal radiologists (R.P. and F.Z.) with expertise in nerve imaging identified the presumed area of the common leash of the PIN. A linear array broadband 17-5MHz US transducer (iU22® platform, Philips Healthcare, Bothell, WA, USA) was used for this purpose. Depending on the examined specimen, the target point was located at the level or just beyond the distal margin of the supinator muscle. The probe was initially placed in an anatomic short-axis plane relative to the PIN fascicles over the distal supinator tunnel. In this location, the PIN consisted of two-three dot-like hypoechoic fascicles sliding into the cleavage plane between the superficial and the deep belly of the supinator muscle. Sweeping the probe downwards, the presumed area of the common leash was assumed to be the point from where the hypoechoic fascicles fan out and diverge. In one specimen, the common leash was injected with 0.2-0.3ml of diluted, red latex (50% water, 50% latex) using a 22 Gauge, 1.5 inch (38mm) stainless steel needle under US guidance. The three elbows were then carefully dissected with the help of an anatomist (M.M.P.) to familiarize with the complexity of PIN arborization and check whether the latex was centered over the common leash. No formal attempt was made to localize the distal divisional branches of the PIN by means of latex injection due to their too tiny size to be reliably marked by such procedure.

Definition of the US Scanning Technique

After the anatomical study, n=20 young (10 females and 10 males, mean age 26 years) healthy volunteers who had BMI in the normal weight (<25) or underweight (<18.5) range were examined with US using an ultra-high frequency, 8mm footprint, 22-8MHz hockey-stick probe (i800 Aplio® platform, Canon Medical Systems, Ōtawara, Japan). None of the volunteers had pain, neurological deficit or other pathologic conditions related to the elbow. In each volunteer, the right and left PIN were systematically examined on short-axis scans while keeping the elbow mildly extended on the table. The wrist-hand was initially oriented palm-up and an anterior approach was selected to firstly recognize the PIN at the level of the radial nerve bifurcation, between the brachialis and the brachioradialis muscles. While sweeping the probe from proximal to distal, progressive degrees of

forearm pronation helped to keep the PIN fascicles centered in the field-of-view of the ultrasound image across the full length of the supinator muscle. With this maneuver, the PIN could be easily followed down beyond the distal edge of the supinator tunnel. In this latter area, the nerve was imaged with the wrist-hand in full pronation, oriented palm-down, and the probe located in a more dorsal position than initially. Probe rotation along the axis, heel-toeing and tilting were used to optimize the conspicuity of the PIN in the area of the common leash. The position of the leash relative to the distal edge of the SSH was classified as either i) intratunnel, ii) at the distal tunnel edge or iii) extratunnel. Particular attention was then directed towards the appropriate scanning technique to image the six divisional branches of the PIN. Using short-axis planes, the number and caliber (diameter) of these small nerves was measured as they diverged from the main PIN trunk. No attempt was made to measure their cross-sectional area as the nerve sizes were too small to enable reliable calculations without introducing systematic errors.

Patients Series

Since February 2015 to August 2022, a series of n=90 consecutive patients (mean age 46±13 years, age range 24-70) with established diagnosis of PIN neuropathy were prospectively examined with high-resolution US in our institution. In each patient, the diagnosis was based on clinical (i.e. finger-drop and variable degree of atrophy of the posterior forearm muscles with exclusion of the brachioradialis, extensor carpi radialis longus and extensor carpi radialis brevis) and/or neurophysiological (i.e. detection of positive sharp waves and/or fibrillation potentials, reduction of motor unit potential amplitude) evidences. Informed consent was obtained from all the patients before the US examination. All the US studies were performed by the same musculoskeletal radiologist (C.M.) who had >20 years of experience in diagnostic US of the musculoskeletal and peripheral nervous systems. A variety of US systems equipped with linear array transducers of different frequency bands were used depending on their availability at the time of examination. They included 17-5MHz and 18-4MHz (iU22® platform, Philips Healthcare, Bothell, WA, USA), 22-8MHz hockey-stick and 24-8MHz (i800 Aplio® platform, Canon Medical Systems, Ōtawara, Japan) probes. Correlative MR imaging was performed in selected cases on either a 1.5T (Magnetom Aero®, Siemens Erlangen, Germany) or a 3-T (Magnetom Prisma®, Siemens Erlangen, Germany) unit using flexible multipurpose RF coils. Variable combinations of sequences and imaging planes were used according to the MR imaging protocols for the PIN described elsewhere (13,14). We excluded from this study patients who had symptoms (i.e. wrist-drop, coexisting sensory deficit in the territory of radial nerve distribution) suggesting a higher level disease involving the main trunk of the radial nerve in the arm or cervical spine disease. Because the clinical and neurophysiological findings are unable to identify the exact level of atraumatic PIN palsy, we categorized our patients in four groups depending on the location of the abnormal nerve segment revealed by US: level #1, from the radial nerve bifurcation down to the proximal edge of the supinator muscle, including the area anterior to the radiocapitellar joint, the recurrent radial vessels that fan out across the PIN at the level of the radial neck and the leading edge of the extensor carpi radialis brevis; level #2, the proximal edge of the supinator muscle (arcade of Frohse); level #3, the supinator tunnel, within which the nerve descends obliquely between the superficial and deep bellies of the muscle; level #4, the distal edge of the supinator muscle or the area immediately beyond it. In this paper we selectively included cases in which the PIN abnormality occurred at level #4. The site of abnormalities encountered in the patient series at level #1 to #3 was, however, recorded to understand the prevalence of level #4 disease. Regarding pathogenesis, there was no attempt to precisely define the cause of PIN palsy and distinguish between mechanical (ie. extrinsic compressive force acting on the nerve) and

nonmechanical (i.e. intrinsic inflammatory reaction within the nerve as it occurs in the Parsonage-Turner syndrome/neuralgic amyotrophy) as differentiation between these two conditions may not be straightforward. In inflammatory conditions, a more extended segment of the nerve is expected to be involved but there is absence of reliable clinical and imaging criteria for such differentiation in the literature. Some attention was instead focused on detection of signs of torsional neuropathy (spontaneous hourglass constriction) with US as a possible cause of PIN dysfunction.

Statistical Analysis

Descriptive statistics were performed using SPSS Statistics for Mac, version 28.0.0 (IBM, Armonk, NY, USA). Metric data (nerve diameter) are presented as mean ± standard deviation (SD) and range (minimum–maximum). Independent sample, unequal variance t-test (Welch's test) was employed to compare the dimension of the distal branches of the PIN.

Results

Cadaveric Study

In the injected specimen, the common leash was depicted on short-axis scans as a flattened hypoechoic area in which the PIN fascicles merged together before diverging into terminal branches. Its visualization was excellent and subsequent dissection confirmed that the injected latex spread around the target (not shown). In all cadaveric specimens, the branching pattern distal to the common leash was quite intricate but, at least in our series, the six terminal divisions supplying the superficial (ie. EDC, EDM, ECU) and deep (ie. APL, EPL, EPB, EIP) muscles of the dorsal forearm were constantly recognized during dissection exposure (Fig.1) .

Normal Ultrasound Findings

In the group of healthy volunteers, the common leash was identified in 31/40 (77.5%) cases as a wide flattened hypoechoic band formed by merging the individual fascicles of the PIN into one complex. In all but one case, the leash was located in the distal third of the supinator tunnel. Its long-axis extension was generally very short and, distally, it split into six terminal branches at the level of the distal boundary of the retinaculum or just beyond it . Although mono-fascicular and sub-millimetric in size, 22-8MHz US was able to image these branches with a high visualization rate . Sweeping the probe down to the leash, the terminal PIN branches split into two major groups of bundles that showed divergent course: ie. a radial bundle, consisting of the #1 to #3 nerves and an ulnar bundles including #4 to #6 nerves (Fig.2) . As a rule, the long branches (ie. #5 and #6) directed to the deep extensor muscles appeared significantly larger ($P<0.01$) than the others and continued the course of the main trunk straight down throughout the dorsal compartment of the forearm. Looking at them from ulnar to radial, high-resolution US detected: the first (#1) winding around the distal boundary of the SSH to reach the EDC muscle with a recurrent course; the second (#2) descended for a short stretch over the SDH before entering the EDC undersurface; the third (#3) and fourth (#4) deflected towards the ulnar side directed towards the ECU and the EDM respectively; the fifth and sixth(#5 and #6) travelled as paired structures straight down in the forearm covered by the EDC, superficial to the SDH (proximally) and the deep layer of the extensor muscles (distally).

Pathological Findings

From our series of n=90 consecutive patients recruited on the basis of clinical and electrophysiological evidence of posterior interosseous neuropathy, high-resolution US was able to recognize pathological findings related to involvement of PIN terminal branches at zone IV in n=13 (14.4%) cases. As assessed with US imaging, these cases included entrapment neuropathies (n=6), traumatic injuries (n=3); space-occupying masses (n=3) and dysimmune neuropathies (n=1). Correlative MR imaging was performed in n=9 of these cases.

Entrapment Neuropathies

In six cases, fusiform swelling of one or more fascicles emerging from the leash was found just beyond the distal edge of the SSH, a pattern that resembled an inverted Frohse . At this landmark, a definite transition between swollen and normal fascicular segments (notch sign) was observed indicating the site of compression. The distal SSH margin appeared more prominent than usual and often revealed a thickened hyperechoic boundary, possibly reflecting fibrotic changes occurring at the distal arcade . One of these patients showed selective compression of the recurrent EDC branch (#1). In this particular case, a fusiform thickening of this small nerve was observed as it circumscribed the distal SSH boundary to move backward and reach the EDC. Selective loss in bulk of the EDC was found relative to the adjacent normally-appearing ECRB and ECU.

Traumatic Injuries

High-resolution US was able to recognize selective damage of the PIN terminal branches in n=3 cases, including two penetrating injuries and one surgical reduction and internal fixation of radial shaft fracture. Meticulous and time-consuming scanning technique was needed to follow the small terminal branches individually across the posttraumatic high-grade derangement of soft-tissues. In our series, nerve injuries occurred just beyond the distal edge of the supinator muscle in two cases and at the mid-forearm in one. When close to the supinator, there was multiple damage of the PIN branches possibly due to their contiguous course, and namely a combined involvement of the #5-#6 and #1,#2,#4-#6 respectively. In the first case, the two severed bundles were embedded in a hypoechoic fibrous scar. In the second, US revealed sparing of the #3 branch as it deflected ulnarly immediately after its origin. Most of the severed nerve bundles were discontinuous without ending in a definite terminal neuroma. Two of them showed a bulbous neuroma measuring 2-3mm in size. In regard to the remaining patient who had mid-forearm injury, an isolated damage of the #6 bundle was demonstrated.

Dysimmune Neuropathy

Selective swelling of the #5 and #6 branches with severe fatty atrophy of the deep extensors was observed beyond the supinator tunnel in a patient with multifocal motor neuropathy and coexisting involvement of the radial nerve in the arm (Fig.3). The abnormal nerve segments extended longitudinally for approximately 4-5cm showing uniform thickening without signs of torsional neuropathy.

Space-Occupying Masses

Two masses associated with selective involvement of the EDC branches were included in our series. The first patient had an intramuscular lipoma of the SDH leading to a high-grade entrapment of the EDC branches against the distal edge of the SSH. In this specific case, it was not feasible to define which EDC nerves (ie. #1, #2 or both) were involved. They looked angled at the muscle boundary and markedly swollen distal to it as a result of compression. The remaining PIN bundles run unaffected alongside the mass. US revealed isolated EDC changes with loss in bulk and hyperechoic pattern of the affected muscle . The second patient had a schwannoma arising from the #2 branch immediately distal to the supinator tunnel. The mass showed a bell-clapper appearance and bulged on the undersurface of the EDC. Similar to the previous case, the remaining nerve bundles were spared and run at the periphery of the mass.

Discussion

Previous anatomical studies showed that the posterior interosseous nerve distal to the supinator muscle may be compressed by various structures. These include the distal border of the supinator muscle, the ramifications of the anterior and posterior interosseous vessels, and the septum between the extensor carpi ulnaris and the extensor digitorum minimi (15,16) The posterior interosseous nerve appeared also stressed during passive supination (elongation and rotation), and during passive pronation (compression) (17).If not considered, entrapment in the more distal regions may be responsible for some of the failures of treatment. Generally initial non-operative treatment of PIN syndrome includes rest, activity modification, and splinting. If no improvement is seen with conservative therapy, patients are usually offered surgery to relieve any extrinsic compression (5).
Regardless of the surgical approaches, transbrachioradialis and anterior approaches are the more frequently used today. Other possible approaches are the dorsal approach between mobile wad and finger extensors (Thompson) and dorsal approach between brachioradialis and wrist extensors (18). All the different surgical techniques start from a point located proximal to the supinator tunnel and then the surgeon proceeds distally, dissecting the PIN; however the surgical access is usually tailored to decompress the nerve at the arcade of Frohse and it may not be wide enough to allow the surgeon to check the distal edge of the tunnel. In a systematic review Huisstede(19) evaluated the effectiveness of surgical decompression of the PIN in patients with PIN syndrome and reported recovery rates of 75%. This review included two studies considered of higher quality, both conducted using an anterior surgical approach (20,21). All the patients of our study underwent electrodiagnostical studies before the US examination and no difference has been revealed between the patients with compression located in zone #2, #3 and #4, with the exclusion of the patient with the partial syndrome caused by the entrapment of the recurrent branch for the extensor digiti communis. All our patients showed typical electrodiagnostical findings of PIN syndrome, with relatively reduced amplitude of motor response of the radial nerve at the affected side (generally recorded from the EIP), normal sensory responses, and denervation signs limited to posterior interosseous-innervated forearm muscles at the electromyography. These data agree with the literature, which reveals that neurophisiology is able to identify a posterior interosseous nerve lesion (differential diagnosis with radial lesions) but fail to define the exact site of the lesion (22-24). In particular, patient with compression at level #1 characteristically show electromyographic abnormality also at the supinator muscle, whereas electromyographic findings of PIN entrapments located at level #2, #3 and #4 are the same. Innervation of the ECRB and the supinator may arise from the proper radial nerve or from the proximal part of the posterior interosseous nerve prior to piercing the supinator muscle, thus the analysis of motor

response of this muscle can not be reliably used in differential diagnosis(23). Moreover, the great variation between subjects in the origin of nerve branches and the number of branches for each muscle is another reason because neurophysiology should be misleading into localizing the PIN lesion(24). On the other hand, ultrasound can exactly recognise the PIN branches injuries, consequently adding important preoperative information to electrodiagnostic studies. Among the patients with PIN compression at the level #4, one showed a partial syndrome with selective enlargement of the recurrent branch of the nerve for the extensor digitorum communis and correlated selective atrophy of the muscle; in our opinion, partial syndromes represent a strong indication for ultrasound examination of the posterior interosseous nerve distal to the supinator because they may be indifferently caused by proximal compression involving only a part of the nerve fascicles or distal damage involving the divisional branch for the affected muscle(22). Finally, high-resolution ultrasound has the potential to disclose double crush syndromes, where the nerve main trunk or its distal branches are compressed at multiple levels but electrodiagnostic studies allow only to identify the most proximal lesion. These conditions may represent a primary cause of failure for nerve decompression procedures and should be systematically ruled out before surgical planning(25).

In our study MRI show an high correlation with US diagnosis and localization of PIN entrapment, showing the typical distribution of muscles edema or atrophy, depending of the duration of entrapment, and thickening of the nerve at the compression point in all the nine cases examined. MRI is also able to provide etiologic information in case of masses or other extrinsic causes of compression. In our experience high-resolution ultrasound examination has some advantage on MRI because it has excellent spatial resolution, dynamic capabilities (i.e. the possibility to explore the nerve during manoeuvre of prono-supination), better availability, low cost and often it is more tolerated by the patient. On the other side MRI offers better panoramic view in the muscle evaluation and the possibility of characterization of PIN compressing masses. Despite the clinical importance of detecting the exact level of entrapment in the context of patients presenting with posterior interosseous neuropathy, no prior study has formally investigated the ability of US to identify selective patology of the PIN at the inferior edge of the superficial belly of the supinator muscle using currently available, high-resolution US probes. Based on our series, the PIN entrapment at the distal edge of the supinator tunnel was found to be relatively common, accounting for approximately 19% of cases. Examiners should therefore include evaluation of the distal tunnel systematically in patients with posterior interosseous neuropathy. Sweeping the probe down beyond the distal edge of the supinator muscle may avoid false negatives. In the preoperative setting, information on the exact location of PIN lesion and release is critical because the surgical access is usually tailored to decompress the nerve at the arcade of Frohse and it may not be wide enough to allow the surgeon to check the distal edge of the tunnel. Ultrasound should therefore be used as an accurate preoperative tool for this purpose because is alble to identify the exact branch of PIN involved corresponding a specific muscle according to a precise somatotopic configuration.

Figure 1

Terminal divisions of the PIN. (A)Cadaveric views and (B)Schematic drawing illustrate the PIN emerging from the supinator tunnel and flattening into a leash (asterisk), before sending its terminal divisions. From ulnar to radial, note the recurrent (#1) and the straight (#2) branches for the extensor digitorum communis (EDC), the ulnarly oriented branch (#3) for the extensor carpi ulnaris (ECU), the thin division (#4) for the extensor digiti minimi (EDM), the fifth branch and its radial (#5 radial) and ulnar (#5 ulnar) distal divisions for the extensor pollicis longus (EPL), the extensor pollicis brevis (EPB) and the extensor indicis proprius (EPI), and the sixth branch (#6), for the abductor pollicis longus (APL), the supinator (SUP) and the EPB. Sensory fibers providing proprioceptive supply to the wrist capsule (WC) can be also found travelling inside the radial division of the fifth branch. BrRad, brachioradialis muscle; ECRB, extensor carpi radialis brevis tendon.

Figure 2

A

B

C

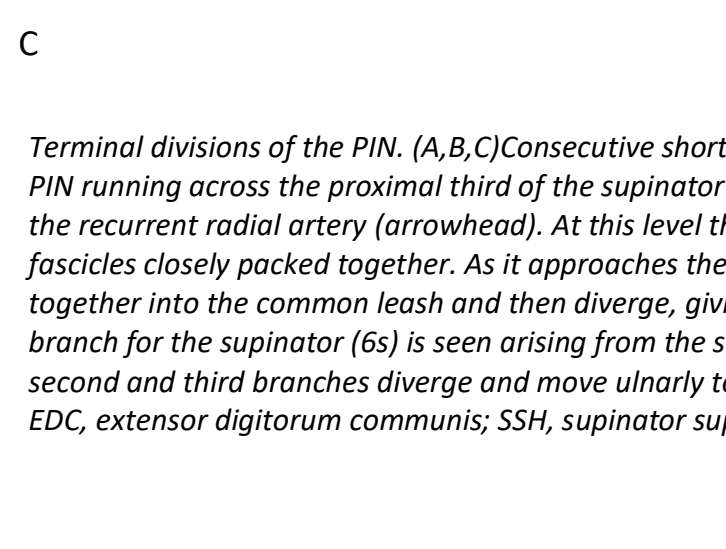

Terminal divisions of the PIN. (A,B,C)Consecutive short-axis 22-8MHz US images demonstrate the PIN running across the proximal third of the supinator tunnel accompanied by a small branch of the recurrent radial artery (arrowhead). At this level the PIN is represented by a small group of fascicles closely packed together. As it approaches the exit of the tunnel, the fascicles firstly merge together into the common leash and then diverge, giving origin to six distinct branches. A motor branch for the supinator (6s) is seen arising from the sixth division of the PIN. More distally, the second and third branches diverge and move ulnarly to reach their distal territories. Rad, radius; EDC, extensor digitorum communis; SSH, supinator superficial head; SDH, supinator deep head.

Figure 3

Inflammatory neuropathy of the fifth and sixth branches of the PIN in a 56 y.o. man with progressive loss of grip strength. Short-axis 17-5MHz US image shows a markedly enlarged fifth (arrow) and sixth (void arrowhead) divisions of the PIN travelling between the deep belly of the supinator (2) and the extensor digitorum communis (EDC). (C)Short axis 17-5MHz US image of the extensor muscle obtained at the middle third of the forearm demonstrates loss in bulk and fatty infiltration selectively affecting the abductor pollicis longus (APL) and the extensor pollicis brevis (EPL) with sparing of the overlying extensor digitorum communis (EDC), extensor digiti minimi (EDM) and extensor carpi ulnaris (ECU) muscles.

References

1. Sunderland S. Nerves and Nerve Injuries. New York: Churchill Livingstone; 1978.
2. Stewart JD. Peripheral nerve fascicles: anatomy and clinical relevance. Muscle Nerve 2003;28:525–541.
3. Pham M, Baumer P, Meinck HM, et al. Anterior interos- seous nerve syndrome: fascicular motor lesions of median nerve trunk. Neurology 2014;82:598–606.
4. Rosenbaum R. Surgical treatment for radial tunnel syndrome. J Hand Surg Am. 1999;24(6):1345-6.
5. Riffaud L, Morandi X, Godey B, et al. Anatomic bases for the compression and neurolysis of the deep branch of the radial nerve in the radial tunnel. Surg Radiol Anat. 1999;21(4):229-33.
6. Konjengbam M, Elangbam J. Radial nerve in the radial tunnel: anatomic sites of entrapment neuropathy. Clin Anat. 2004;17(1):21-5.
7. Clavert P, Lutz JC, Adam P, Wolfram-Gabel R, Liverneaux P, Kahn JL. Frohse's arcade is not the exclusive compression site of the radial nerve in its tunnel. Orthop Traumatol Surg Res. 2009;95(2):114-8.
8. Liotta G, Granata G, Librante A, et al. Atypical double nerve lesion after humeral fracture: diagnosis by ultrasound. Muscle Nerve. 2010;41(2):287-8.
9. Prasartritha T, Liupolvanish P, Rojanakit A. A study of the posterior interosseous nerve (PIN) and the radial tunnel in 30 Thai cadavers. J Hand Surg Am. 1993;18(1):107-12.
10. Lister GD, Belsole RB, Kleinert HE. The radial tunnel syndrome. J Hand Surg Am. 1979;4(1):52-9.
11. Ay S, Apaydin N, Acar H, et al. Anatomic pattern of the terminal branches of posterior interosseous nerve. Clin Anat. 2005;18(4):290-5.
12. Elgafy H, Ebraheim NA, Rezcallah AT, Yeasting RA. Posterior interosseous nerve terminal branches. Clin Orthop Relat Res. 2000;(376):242-51.
13. Spinner RJ, Berger RA, Carmichael SW, Dyck PJB, Nunley JA. Isolated paralysis of the extensor digitorum communis associated with the posterior (Thompson) approach to the proximal radius. J Hand Surg Am. 1998;23(1):135-41.
14. Chien AJ, Jamadar DA, Jacobson JA, Hayes CW, Louis DS. Sonography and MR imaging of posterior interosseous nerve syndrome with surgical correlation. AJR Am J Roentgenol. 2003;181(1):219-21.
15. Bodner G1, Harpf C, Meirer R, Gardetto A, Kovacs P, Gruber H. Ultrasonographic appearance of supinator syndrome. J Ultrasound Med. 2002;21(11):1289-93.
16. Sponseller PD, Engber WD. Double-entrapment radial tunnel syndrome. J Hand Surg Am. 1983;8(4):420-3.
17. Portilla Molina AE, Bour C, Oberlin C, Nzeusseu A, Vanwijck R. The posterior interosseous nerve and the radial tunnel syndrome: an anatomical study. International Orthopaedics. 1998;22(2):102-6.
18. Moradi A, Ebrahimzadeh MH, Jupiter JB. Radial Tunnel Syndrome, Diagnostic and Treatment Dilemma. Arch Bone Jt Surg. 2015;3(3):156-62.

19. Huisstede BM, Miedema HS, van Opstal T, et al. Interventions for treating the posterior interosseus nerve syndrome: a systematic review of observational studies. J Peripher Nerv Syst. 2006;11(2):101-10.
20. Vrieling C, Robinson P. Geertzen, J. Posterior interosseous nerve syndrome: literature review and report of 14 cases. E J Plastic Surg. 1998;21:196-202.
21. Kalb K, Gruber P, Landsleitner B. Non-traumatically-induced paralysis of the ramus profundus nervi radialis. Aspects of a rare disease picture. Handchir Mikrochir Plast Chir. 2000;32(1):26-32.
22. Lawley AR, Saha S, Manfredonia F. Posterior interosseous neuropathy: the diagnostic benefits of a multimodal approach to investigation. Clin Case Rep. 2016;4(4):437-41.
23. Bevelaqua AC, Hayter CL, Feinberg JH, Rodeo SA. Posterior interosseous neuropathy: electrodiagnostic evaluation. HSS J. 2012;8(2):184-9.
24. Borman P, Tuncay F, Ulusoy G, Koçer U. Posterior interosseous nerve syndrome due to lipoma. Neurophysiol Clin. 2010;40(3):189-91.
25. 25. Dietz AR, Bucelli RC, Pestronk A, Zaidman CM. Nerve ultrasound identifies abnormalities in the posterior interosseous nerve in patients with proximal radial neuropathies. Muscle Nerve. 2016;53(3):379-83.

Recurrent motor branch neuropathy in carpal tunnel syndrome: an ultrasound and electrophysiological study

in collaboration with Professor Maribel Miguel Pérez, Unidad de Anatomía y Embriología Humana, Departamento de Patología y Terapéutica Experimental, Universidad de Barcelona

Carpal tunnel syndrome (CTS) is the most common entrapment neuropathy with a reported prevalence in the general population ranging from 1% to 5%[1-3]. Sensory symptoms like tingling, paresthesia and burning pain at the palmar aspect of the first three and half fingers represent the usual presentation of the syndrome, whereas advanced cases are characterized by the onset of motor deficit, with thenar eminence muscles atrophy and consequent progressive loss of thumb abduction and opposition. Sensory disturbances are thought to precede motor impairment due to a relative increased susceptibility to ischemia of sensory axons, which demonstrate faster depolarization and early inactivation of Na+ channels following prolonged compression[4]. The recurrent motor branch (RMB) is a small but clinically relevant division of the median nerve (MN) that supplies the muscles of the thenar eminence (i.e., opponens pollicis, abductor pollicis brevis and superficial belly of the flexor pollicis brevis), thus being responsible for most of the motor function of the thumb[5-7]. Although RMB neuropathy most commonly follows iatrogenic damage during surgical carpal tunnel release, compression injuries have been hypothesized to accelerate the progression of thenar muscles wasting in a subset of patients with CTS[8-11]. Anatomical variations of RMB origin and course have been sporadically suggested to expose the nerve at an increased risk of impingement, but to date the occurrence and the ultimate role of RMB neuropathy in patients with CTS have not been elucidated[12,13]. High-resolution ultrasound (US) has shown its potential to demonstrate the RMB, disclose the presence of anatomical variations and characterize morphological changes in case of nerve pathology[14-16]. Accordingly, the aim of this study was to evaluate the occurrence of US signs of RMB neuropathy in a cohort of patients with CTS and thenar muscles denervation and to correlate imaging findings with clinical and electrophysiological tests.

Anatomical considerations

The anatomical course of the RMB has been extensively investigated in the past due to its clinical relevance and the relative frequency of iatrogenic injury during carpal tunnel surgery[1-3]. In most instances (extraligamentous or type-I variant Lanz's classification), after originating from the MN at the distal carpal tunnel, the RMB points to the palm (*first* or *vertical tract*), bends around the distal edge of the flexor retinaculum and takes a retrograde course across the muscles of the thenar eminence (*second* or *horizontal tract*) (Fig. 1). Anomalous paths are encountered in around 11% of people: the RMB may arise proximally within the carpal tunnel and then run underneath the flexor retinaculum alongside the MN (i.e subligamentous path or type-II variant) or may exit the carpal tunnel piercing the thickness of the retinaculum (i.e. transligamentous or type-III variant)[17]. In addition, the RMB may arise from the MN as a single or multiple branches, may be variably oriented after branching from the MN or may be overlayed by anomalous structures[18,19]. Finally, there is poor agreement about the mean transverse diameter of the RMB, with reported values ranging between 0.7 to 3 millimeter[14,15].

Materials and Methods

Approval for this multicentric study, performed at IRCCS Ospedale Policlinico San Martino (Genoa, Italy) and at the Ospedale San Andrea (La Spezia, Italy) was obtained from the competent Ethics Committee (Comitato Etico Regione Liguria, protocol code 12637, approved on 07/10/2022). Following informed consent, two cohorts were enrolled, respectively consisting of patients from the Neurophysiology Unit of the Ospedale San Andrea with electrophysiological evidence of CTS and altered median distal motor latency from wrist to thenar eminence (DML) and sex- and age-matched volunteers from the Radiology Unit of the IRCCS Ospedale San Martino without clinical evidence or history of CTS. Exclusion criteria for the two cohorts consisted of: i) diagnosis of polyneuropathy and ii) previous surgical procedures or major trauma around the wrist.

Clinical and Electrophysiological evaluation of patients

All the patients were requested to fulfill the Boston Carpal Tunnel Questionnaire (BCTQ), which provides a standardized graduation of symptoms and functional status and has been demonstrated to represent a valid primary outcome measure in CTS trials[20]. The BCTQ evaluates two domains of CTS: ‘‘symptoms” (SYMPT = patient-oriented symptoms) assessed on a 11-step scale; and ‘‘functional status” (FUNCT = patient-oriented function) assessed on an 8-step scale. Each item includes five possible responses, and the score for each section (SYMPT and FUNCT) is calculated as the mean of the responses to the individual items. In addition, the motor function of patients was evaluated and scored through the Medical Research Council (MRC) Scale[21]. Neurophysiological studies were conducted the same day of the US examination, according to accepted clinical standards[22]. The skin temperature was maintained at ≥ 32 °C throughout the study and nerve conduction was measured orthodromically by means of superficial stimulation and recording. First-line tests included: i) MN sensory conduction velocity (SNCV) from first digit to wrist (1M); ii) MN SNCV from third digit to wrist (3M); iii) MN DML from wrist to thenar eminence; iv) radial nerve SNCV from first digit to wrist (1R). As recommended by the American Association of Electrodiagnostic Medicine[23], when first-line tests yielded normal results, more sensitive studies (distal to proximal ratio), aimed at excluding subtle or initial neuropathies, were carried out as follows: i) MN SNCV from third digit to palm (3P); ii) MN SNCV from palm to wrist (P-W) calculated as 3M-3P; iii) the distal to proximal ratio (R) calculated as 3P/(P-W). Extended sensory and motor nerve conduction studies of the ulnar nerve were also carried out to exclude polyneuropathy.

Patients were divided into six groups (i.e., negative test or extreme, severe, moderate, mild and minimal CTS) according to accepted neurophysiological classification of CTS severity[24]. Patients with at least moderate CTS (DML≥4ms or undetectable motor responses) were included in the study and submitted to US evaluation.

Ultrasound examination and scanning technique in healthy volunteers

In volunteers, the RMB diameter was measured by two radiologists (F.Z and R.P) with respectively n:7 and n:5 years of experience in the field of musculoskeletal US using linear, high-frequency, matrix array 18-5MHz transducer and an ultra-high frequency, 8mm footprint, 22-8MHz hockey-stick probe (Aplio i800 platform, Canon Medical Systems, Ōtawara, Japan). All the volunteers were examined twice by one assessor, with seven days elapsing between the two measurements, and once by the second assessor, who was unaware of the other observer's results. The RMB was firstly recognized as a thin fascicular structure running over the palmar surface of the flexor pollicis brevis and then was tracked toward distal until it was seen rejoining with the MN (Fig. 2). In doubtful cases or when it was not possible to identify the RMB along its usual path, the detection was attempted following the MN from proximal to distal along the carpal tunnel and trying to identify the RMB at its origin. The RMB diameter was measured shortly after branching from the MN at the level of the vertical tract. Transducer rotation on the RMB long axis, heel-toeing and tilting were used to optimize the visualization of the nerve and reduce artifacts related to anisotropy.

Ultrasound examination in patients

All the patients were evaluated by a single operator and the RMB diameter was measured at the level of the vertical tract as described in the previous section. In addition, the following parameters were collected: i) MN cross-sectional area at the level of the proximal carpal row; ii) MN cross-sectional area at the distal carpal row; iii) thickness of the flexor retinaculum. In addition, flexor tendon tenosynovitis along the carpal tunnel and thenar muscles atrophy were subjectively graded in four classes (i.e., absence, mild, intermediate, or severe). Thenar muscles trophism was evaluated based on muscles echogenicity and volume, using as a reference the trophism of the flexor digitorum superficialis at the mid forearm. Finally, predominant MN compression was defined as occurring at the proximal or distal part of the carpal tunnel considering the area of maximal nerve enlargement along its course across the tunnel itself.

Statistical analysis

Mean value and standard deviation were reported as descriptive values for continuous variables, while categorical variables were reported as frequencies (percentages). After verification of normality, comparison of demographic and clinical characteristics between study groups were assessed using T-test for independent groups or Chi-square test, as appropriate. The intra- and inter-observer reliabilities in US measurement of RMB diameter were established by calculating the intra-class correlation coefficient (ICC) and its 95% confidence interval (CI) using an absolute agreement, two-way random effect model. ICC values below 0.20 were interpreted as poor reliability, from 0.21 to 0.40 as fair reliability, from 0.41 to 0.60 as moderate reliability, from 0.61 to 0.80 as good reliability and from 0.81 to 1 as very good reliability. In patients, the association between RMB diameter and other clinical, electrophysiological and US data was assessed by means of a linear mixed model with RMB diameter as dependent variable and unstructured

covariance matrix. All data processing steps and statistical analysis was performed in SAS version 9.4 (Institute Inc., Cary, NC, USA).

Results

Study populations

Demographic characteristics of the investigated cohorts are shown in Table 1. A total of 46 hands (26 right, 56.4%) from 32 patients (13 males, 40.6%; average age 62.3±12.6 years) with CTS were evaluated in the period between January 12, 2018 and February 22, 2023. 29 patients (90.6%) were right-handed and CTS symptoms duration averaged 24.0±32.2 months. According to electrophysiology CTS was classified as moderate, severe, and extreme in respectively 38, 5, and 3 hands. In 71.7% of patients the clinical exam demonstrated regular thenar muscles strength (MRC=5) whereas 28.3% of patients were graded MRC=4. This cohort was matched for sex, age, and BMI to 50 volunteers (22 males, 44.0%; 45 (90.0%) right-handed) without clinical evidence of CTS (average age 61.4 ± 12.5 years).

Ultrasound, clinical and electrophysiological evaluation

Table 2 and Table 3 respectively show US, clinical, and electrodiagnostic results obtained in the patients' cohort and their correlation with RMB diameter. US allowed the identification of the RMB in the totality of patients and volunteers. In both the cohorts, the nerve was constantly found running on the palmar surface of the distal part of the flexor pollicis brevis and, from this point, was tracked back until its origin from the MN. In 4 out of 96 hands (4,1%), the RMB was appreciated detaching from the MN inside the carpal tunnel and then running parallel to it until the distal edge of the retinaculum. Overall, it was not possible to reliably establish if at this level the RMB pierced the most distal part of the retinaculum or bended around the distal edge to reach the thenar musculature.
The intra- and interobserver agreements in RMB measurement resulted very good (ICC 0.84, 95%CI: 0.75-0.90) and good (ICC 0.79, 95%CI 0.69-0.87) respectively, confirming the reliability of US in the evaluation of this small nerve. The mean of RMB diameter at the level of the vertical tract in patients resulted significantly larger compared to the RMB diameter in volunteers (0.97 vs 0.69, p<.0001). In patients, the RMB diameter was significantly associated to BMI (β=0.02, 95%CI: 0.004 -0.04), distal MN cross sectional area (β=0.02, 95%CI: 0.005-0.04) and proximal MN cross sectional area (β=0.02, 95%CI: 0.0005-0.04). In 17 out of 46 (36.96%) the MN resulted maximally enlarged at the level of the distal carpal tunnel, in relation to a predominant compression against the distal edge of the flexor retinaculum. However, the RMB diameter was not found significantly different between cases with proximal (M=0.95 mm, SD=0.31 mm) and distal (M=1.00 mm, SD=0.29 mm) MN compression (p=0.960, derived from a mixed model, which was applied in order to consider inter-hand correlation).

Discussion

In the present study, high-resolution US has been demonstrated to be accurate and reproducible in measuring RMB diameter at the level of the vertical tract, with intra- and interobservers agreement respectively rated very good and good. In our cohort, the RMB diameter averaged 0.69mm (SD=0.14mm), strongly matching with the results presented in a recently published US

study[15]. In addition, a statistically significant enlargement of the RMB was demonstrated in patients affected by CTS and altered DML (Fig. 3). In compression neuropathies, US demonstration of nerve swelling is related to the impaired venous drainage and the progressive accumulation of intraneural fluids caused by the increased pressure on the vasa nervorum. In this view, US allowed to detect signs of RMB edema in patients with CTS and altered DML, thus showing potential in providing evidence of motor damage in this cohort. Notably in our series of patients RMB diameter was not found correlating with any clinical or neurophysiological parameter, whereas a significant positive correlation was found with BMI and MN cross sectional area, this latter measured both at the proximal and distal edge of the flexor retinaculum. Even if the association between nerve diameter and BMI has already been evidenced in previous studies[25], at the best of our knowledge the correlation between MN and RMB diameters has not been reported yet. On the other hand, the absence of correlation between RMB diameter, patient 's symptoms, and neurophysiological class may have different explanation. First, nerve enlargement may be not proportional to the severity of compression, as peripheral nerve may shrink in very advanced syndromes due to the occurrence of intraneural fibrotic changes[26]. Then, in Padua's classification an upgrade from grade 3 to grade 4 is only driven by a worsening of the sensory function and doesn't require any aggravation of the motor function. In addition, DML doesn't show a linear growth in advanced grades of CTS severity, as it tends to raise from mild to severe cases, but it is not calculable in extreme CTS, that are characterized by absence of motor axon conduction. The positive correlation between RMB diameter and MN CSA demonstrates that the edematous changes found in this distal division are more prominent in cases where the main nerve trunk is more severely swollen at the level of the carpal tunnel. This may be explained considering that axons edema in compression neuropathies is maximal around the compression point but tends to persist few centimeters proximal or distal to it, and the motor axons compressed inside the carpal tunnel may show signs of nerve edema also after having branched from the main nerve trunk (Fig. 4). However, we didn't find any difference of RMB diameter between patients with prevalent proximal or distal compression, suggesting the absence of an additional risk of RMB edema in cases where the MN is more prominently compressed around the origin of the RMB itself. In addition, also the thickness of the flexor retinaculum and the presence of flexor tendons tenosynovitis were not significantly linked to the degree of RMB swelling. Overall, we were not able to demonstrate a single anatomic factor determining a more prominent RMB edema other than the degree of MN swelling. However, we cannot exclude that minor anatomical variations not detected by US such as anomalous carpal tunnel shapes or abnormal and inhomogeneous thickening of the flexor retinaculum may determine in some patients a redistribution of the pressure forces exerted against the MN and predispose motor fascicles to an earlier and more pronounced damage. In addition, variation in the fascicular topography of the MN at the level of the carpal tunnel may contribute to explain the multifaceted clinical course of CTS, with more severe motor impairment occurring in cases where motor fascicles are in close contact with the retinaculum or in areas of the nerve more subject to compression and ischemia[27]. At the end, we cannot exclude the existence of a subgroup of patients with CTS predisposed to early thenar muscle denervation as a consequence of local anatomic factors. We recognize that our study presents several limitations. Firstly, we were able to include only a small sample of patients with CTS. Larger and multicenter studies are needed to confirm our results. Finally, we didn't include any patients with mild CTS and normal motor conduction tests. Consequently, we cannot assume the existence of any difference between the RMB involvement in patients with or without thenar muscles denervation changes detected at electrodiagnostic tests. In conclusion, high-resolution US is reliable in identifying the RMB of the MN and characterizing its abnormalities. In patients with CTS and altered DML, US allowed the detection of definite signs of RMB compression neuropathy.

Prospective studies are needed to investigate if the identification of RMB edema by means of high-resolution US indicates an additional risk of CTS progression and may play a role in addressing high-risk patients to prompt carpal tunnel release.

References

1. Seror P. Sonography and electrodiagnosis in carpal tunnel syndrome diagnosis, an analysis of the literature. Eur J Radiol 2008;67:146-152.
2. Martinoli C, Bianchi S, Gandolfo N, Valle M, Simonetti S, Derchi LE. US of nerve entrapments in osteofibrous tunnels of the upper and lower limbs. RadioGraphics 2000;20:199-213.
3. Buchberger W, Judmaier W, Birbamer G, Lener M, Schmidauer C. Carpal tunnel syndrome: diagnosis with high-resolution sonography. AJR Am J Roentgenol 1992;159(4):793-798.
4. Hofmeijer J, Franssen H, van Schelven LJ, van Putten MJ. Why are sensory axons more vulnerable for ischemia than motor axons? PLoS One. 2013 Jun 20;8(6):e67113.
5. Ajmani ML. Variations in the motor nerve supply of the thenar and hypothenar muscles of the hand. J Anat 1996;189:145-150.
6. Alp M, Marur T, Akkin SM, Yalcin L, Demirci S. Ramification pattern of the thenar branch of the median nerve entering the thenar fascia and the distribution of the terminal branches in the thenar musculature: Anatomic cadaver study in 144 hands. Clin Anat 2005;18:195-199.
7. Samarakoon LB, Guruge MH, Jayasekara M, Malalasekera AP, Anthony DJ, Jayasekara RW. Anatomical landmarks for safer carpal tunnel decompression: an experimental cadaveric study. Patient Saf Surg 2014;8(1):8.
8. Tate DE Jr. Isolated fascial compression of the recurrent motor branch of the median nerve: A case report. Hand (N Y) 2006;1:102-105.
9. Shams OE, Al-Ghamdi SM. Isolated neuropathy of the recurrent motor branch of the median nerve. Neurosciences 2006;11:326-328.
10. Rizzello G, Longo UG, Franceschi F, et al. Compression neuropathy of the motor fibers of the median nerve at wrist level. J Chin Med Assoc 2009;72(5):268-270.
11. Kobayashi N, Koshino T, Nakazawa A, Saito T. Neuropathy of motor branch of median or ulnar nerve induced by midpalm ganglion. J Hand Surgery 2001;26(3):474-477.
12. Johnson RK, Shrewsbury MM. Anatomical course of the thenar branch of the median nerve usually in a separate tunnel through the transverse carpal ligament. J Bone Joint Surg Am 1970;52(2):269-273.
13. Wolf AW, Packard S, Chow JC. Transligamentous motor branch of the median nerve discovered during endoscopically assisted carpal tunnel release. Arthroscopy 1993;9:222-223.
14. Smith J, Barnes DE, Barnes KJ, Strakowski J, Lachman N, Kakar S, Martinoli C, Sonographic Visualization of Thenar Motor Branch of the Median Nerve: A Cadaveric Validation Study. PM R 2017;9(2):159-169.
15. Riegler G, Pivec C, Platzgummer H, Lieba-Samal D, Brugger P, Jengojan S, Vierhapper M, Bodner G. High-resolution ultrasound visualization of the recurrent motor branch of the median nerve: normal and first pathological findings. Eur Radiol 2017;27:2941-2949 .

16. Petrover D, Bellity J, Vigan M, Nizard R, Hakime A. Ultrasound imaging of the thenar motor branch of the median nerve: a cadaveric study. Eur Radiol 2017;27:4883–4888.
17. Lanz U. Anatomical variations of the median nerve in the carpal tunnel. J Hand Surg Am 1977;2(1):44-53.
18. Schultz RJ, Endler PM, Huddleston HD. Anomalous median nerve and an anomalous muscle belly of the first lumbrical associated with carpal-tunnel syndrome. J Bone Joint Surg Am 1973;55(8):1744-1746.
19. Henry BM, Zwinczewska H, Roy J, Vikse J, Ramakrishnan PK, Walocha JA, Tomaszewski KA. The Prevalence of Anatomical Variations of the Median Nerve in the Carpal Tunnel: A Systematic Review and Meta-Analysis. PLoS One 2015;25,10(8):e0136477.
20. Leite JC, Jerosch-Herold C, Song F. A systematic review of the psychometric properties of the Boston Carpal Tunnel Questionnaire. BMC Musculoskelet Disord 2006;7:78.
21. Paternostro-Sluga T, Grim-Stieger M, Posch M, et al. Reliability and validity of the Medical Research Council (MRC) scale and a modified scale for testing muscle strength in patients with radial palsy. J Rehabil Med 2008;40(8):665-671.
22. Jablecki CK, Andary MT, Floeter MK, et al. Practice parameter: Electrodiagnostic studies in carpal tunnel syndrome. Report of the American association of electrodiagnostic medicine, American academy of neurology, and the American academy of physical medicine and rehabilitation. Neurology 2002;58(11):1589-1592.
23. AAEM Quality Assurance Committee. Literature review of the usefulness of nerve conduction studies and electromyography for the evaluation of patients with carpal tunnel syndrome. Muscle Nerve 1993;16:1392-1414.
24. Padua L, Lo Monaco M, Padua R, Gregori B.Tonali P. Neurophysiological classification of carpal tunnel syndrome: assessment of 600 symptomatic hands. ItaL J Neurol Sci 1997;18:145-150.
25. Werner RA, Jacobson JA, Jamadar DA. Influence of body mass index on median nerve function, carpal canal pressure, and cross-sectional area of the median nerve. Muscle Nerve 2004;30:481-485.
26. Mulroy E, Pelosi L. Carpal tunnel syndrome in advanced age: A sonographic and electrodiagnostic study. Muscle Nerve 2019;60:236-241.
27. Planitzer U, Steinke H, Meixensberger J, Bechmann I, Hammer N, Winkler D. Median nerve fascicular anatomy as a basis for distal neural prostheses. Ann Anat 2014;196:144-9.

Abbreviations:

RMB: Recurrent Motor Branch

MN: Median Nerve

CTS: Carpal Tunnel Syndrome

US: Ultrasound

SNCV: Sensory Conduction Velocity

DML: Distal Motor Latency

Tables

Table 1: Demographics of the investigated cohort and RMB diameter.

§ p-value derived from a mixed model, which was applied in order to consider inter-hand correlation

* number of observations/number of patients

	Patients	***Volunteers***	***p-value***
N	46/32*	50	
Gender, n(%)			0.707
Female	19 (59.38)	28 (56.00)	
Male	13 (40.63)	22 (44.00)	
Age (years), mean (SD)	62.31 (12.63)	61.36 (12.55)	0.826
BMI, mean (SD)	24.99 (4.68)	24.22 (2.93)	0.713
Hands, n(%)			0.763
Right	26 (56.42)	30 (60.00)	
Left	20 (43.48)	20 (40.00)	
Right-handed, n(%)	29 (90.63)	45 (90.00)	0.926
Duration of sympthoms (month), mean (SD)	24.03 (32.21)		
RMB diameter	0.97 (0.30)	0.69 (0.14)	<.0001§

Table 2: US, clinical, and electrophysiological results in patients' cohort.

	Mean	***SD***
BCTQ FUNCT	2.31	0.83
BCTQ SYMP	2.86	0.72
SNCV	32.44	12.61
DML	5.51	2.25
Proximal MN CSA	13.70	5.00
Distal MN CSA	12.18	4.71
Thickness of retinaculum	0.87	0.22
Tenosynovitis		
Absence 29 (63%)		
Mild 16 (34.8%)		
Moderate 1 (2.2%)		
Severe 0 (0%)		
Thenar muscle atrophy		
Normal 37 (80.4%)		
Mild 5 (10.9%)		
Moderate 4 (8.7%)		
Severe 0 (0%)		
Neurophysiological class		
Moderate 38 (82.7%)		
Severe 5 (10.8%)		
Extreme 3 (6.5%)		

Table 3. US, clinical and electrophysiological variables associate with RMB diameter.

	β Coefficients (95%CI)	***p-value***
BMI	0.02 (from 0.004 to 0.04)	**0.021**
BCTQ FUNCT score	0.03 (from -0.09 to 0.14)	0.627
BCTQ SYMP score	0.005 (from -0.12 to 0.13)	0.941
MRC scale	-0.04 (from -0.24 to 0.16)	0.672
Duration of symptoms	0.001 (from-0.002 to 0.003)	0.608

Neurophysiologic class	0.09 (from -0.05 to 0.24)	0.197
GISSTC	-0.004 (from-0.17 to 0.16)	0.959
SNCV	-0.003 (from-0.01 to 0.004)	0.431
DML	0.01 (from -0.04 to 0.07)	0.675
Proximal MN CSA	0.02 (from 0.005 to 0.04)	**0.015**
Distal MN CSA	0.02 (from 0.0005 to 0.04)	**0.044**
Thickness of flexor retinaculum	0.09 (from -0.32 to 0.50)	0.673
Thenar muscle atrophy	0.01 (from -0.14 to 0.16)	0.876
Tenosynovitis	-0.01 (from -0.18 to 0.16)	0.890

Figure 1

Schematic drawing shows the anatomy of the recurrent motor branch. In the first or vertical tract (black arrowhead), the nerve abruptly points toward the palm immediately after its origin from the radial division of the median nerve (black arrow). It then bends around the distal edge of the flexor retinaculum (FR) and runs horizontally (outlined arrowhead, second or horizontal tract) at first over the palmar surface of the flexor pollicis brevis (FPB), and then in the interstitium between the opponens pollicis (OP) and abductor pollicis brevis (ApB). Outlined arrow, ulnar division of the median nerve; FPL, flexor pollicis longus.

Figure 2

Recurrent motor branch normal anatomy. (A)Distal and (B) proximal short-axis 22-8MHz US images and (C)long-axis 22-8MHz US image obtained at the level of the thenar eminence demonstrate the course of the recurrent motor branch of the median nerve (arrowhead). In (A) the nerve is shown at the vertical tract short after its origin from the radial division of the median nerve (arrow). In (B) the recurrent motor branch is demonstrated at the horizontal tract, over the ventral surface of the superficial head of the flexor pollicis brevis muscle (FPBsh). Void arrow, ulnar division of the median nerve; AdP, adductor pollicis; OP, opponens pollicis; FT, flexor tendons.

Figure 3

Recurrent motor branch compression neuropathy in a 68 year old male patient with carpal tunnel disease. Transverse 22-8MHz US image demonstrates an enlarged recurrent motor branch (arrowhead) arising from the radial division of the median nerve (arrow). Note the increased echogenicity of the superficial head of the flexor pollicis brevis (FPBsh) compared to the normal-echogenic adductor pollicis (AdP), in relation to moderate atrophic changes affecting the first. Void arrow, ulnar division of the median nerve; FT, flexor tendons.

Figure 4

Recurrent motor branch neuropathy in a 74 year old male patient with predominantly distal median nerve compression. (A) Short-axis 18-5MHz US image obtained at the level of the scaphoid (Sca) and pisiform (Pis) bones demonstrates a moderately enlarged median nerve (white arrows) running between the flexor retinaculum (void arrowheads) and the flexor tendons (FT). (B) Short-axis 18-5MHz US image obtained at the distal carpal tunnel shows the abrupt flattening of the median nerve (white arrows) as it passes underneath the thickened distal part of the flexor retinaculum (arrowheads). Note the origin of the abductor pollicis brevis (AbP) and of the opponens pollicis (OP) from the retinaculum and the trapezium (Tra). Pis, pisiform. (C) Short-axis 18-5MHz US image demonstrates edematous changes affecting the vertical tract of the recurrent motor branch. Note the markedly swollen ulnar (void arrow) and radial (black arrow) divisions of the median nerve and the anomalous origin of the recurrent motor branch from the first. FPBsh, superficial head of the flexor pollicis brevis; AdP, adductor pollicis. (D) Long-axis 18-5MHz US image of the median nerve shows the inverted notch sign (arrowheads), with significant swelling and hypoechogenicity of the median nerve at the distal carpal tunnel (void arrows) and almost normal nerve appearance at the proximal tunnel (arrows), in relation to predominantly distal nerve compression. Ft, flexor tendons.

Magnetic Resonance Imaging (MRI) phenotyping of muscle and nerve in a mouse model of Charcot-Marie-Tooth type 1B neuropathy using a 7Tesla systema: a pilot study

Background and rationale

Mutations in the Myelin Protein Zero gene (MPZ) are the cause of Charcot-Marie-Tooth (CMT) type 1B neuropathy. We recently generated a mouse model carrying the MPZD61N mutation (1), causing in humans a severe early onset form of CMT1B. MPZD61N/+ mice develop a tremor as early as P15, which worsens with age and correlates with a significant motor impairment, reduced muscular strength and with substantial alterations in neurophysiology. Some authors previously identified components of both the innate and the adaptive immune system as disease modifiers in the pathogenesis of models for Charcot-Marie-Tooth (CMT) neuropathies type 1B,1X and 1a (2).

MRI imaging is routinely used in clinical practice to study and monitor neuromuscular disorders, in particular to demonstrate nerve alterations and muscle neurogenic changes. Concerning nerve alterations, the standard sequence protocol includes 3D T2 weighted with Inversion Recovery and the recently included DTI with evaluation of Fractioned Anisotropy (3). Regarding muscle, Dixon sequences with chemical-shift fat-water separation enable the quantification of intramuscular fat as biomarker of muscle atrophy. However, T1-mapping sequences are still poorly investigated as biomarker of muscle degeneration in neuromuscular disease, since T1 in muscle tissue is not only related to the fat content but may be influenced by muscle edema, cellular depletion or increased extracellular space (4,5). So far the relation between the entity of macrophages infiltrate at level of muscle and nerve and changes in MR parameters have not been indagated yet.

By using a dedicated MRI 7T system, here we aimed at monitoring the progressive nerve and muscle damage in hetero- and homozygous knock-in mice. We also indagated the histopathological correlation of nerve and muscle signal alterations, with a specific focus on the influence of the innate imminity cell infiltrate on the quantitative MR parameters.

Materials and Methods

We analyzed three groups of animals,(WT , MPZD61N/+ and MPZD61N/MPZD61N), 6 animals for each group age and sex matched utilizing a 7T MRI system (Pharmascan, Bruker). Animals were anesthetized and placed prone in a dedicated whole-body coil, keeping the hindlimbs fully extended and fixed to the bed. An additional phased array, 8-channel, surface coil was positioned over the bilateral thigh. A 45 minutes protocol was applied (see below). Quantitative parameter as T1 echo time of the thigh muscle, T2* echo time of the sciatic nerve and thigh muscle and Fractioned Anisotropy (FA) of the sciatic nerve were obtained utilizing the software Paravision 360. For the comparison of the mean scores of T1_muscle, T2_muscle, T2_nerve and FA in the specific groups, we used one-way analysis of variance (ANOVA). For the data which meet the assumption of the homogeneity of variance, we applied post-hoc Hochberg's GT2 test, while with reference to data which do not meet this assumption, we applied the Games–Howell test. The results were analyzed using the SPSS Statistics vs. 21.0. program for Windows. The level of significance for tests was set at a p value < 0.05. Folllowing MR examination, animals were sacrificed, and thigh muscle tissue and sciatic nerve were harvested and formalin-fixed for histological analysis. In order to assess the inflammatory status of mutant nerves, we immunostained WT, MpzD61N/+ and Mpz-D61N/D61N sciatic nerves for Myeloperoxidase (MPO) and F4/80. The presence of muscle atrophy with fibroadipose infiltration was also evaluated after standard Hematoxylin-Eosin staining

Sequence	Repetition/ echo time (ms)	Flip angle (degrees)	Slice thickness (mm)	Slice gap (mm)	Field of View (mm)	Matrix	Acquisition time
T2 RARE Inv Rec	10.000/37	90	0,8	0,3	41,565 x 41,617	384 x 512	8m
DTI EPI 30 dir	2.500/35	90	0,8	0,3	41,565 x 41,617	96 x 96	2m55s
T2* map MGE	1.157,229/4-39 (n=8)	50	0,8	0,3	41,565 x 41,617	256 x 256	7m24s375ms
T1 map RARE	5.500-504 (n=6)/8	90	0,8	0,3	41,565 x 41,617	256 x 256	18m53s598ms

Table 1. Parameters of the sequences included in the MRI protocol

Results

We found that FA was significantly lower (P = 0.01) in MPZD61N/MPZD61N mice compared with MPZD61N/+ and WT littermates. Nerve T2* progressively increased from WT to MPZD61N/MPZD61N, but the statistical difference between values was not reached. The decreased fractioned anisotropy is representative of the histological de-structuration of myelin envelop as seen at the electronic microscopy, whit loss of directionality of water molecules motion within the axons. Interestingly, we found an increased density of inflammatory cells in mutant mice, compared with WT mice. Notably, $Mpz^{D61N/D61N}$ mice showed the higest density of positive cells, suggesting that inflamatory infiltration correlates with disease severity.The tendency of nerve T2star signal to increase from wildtype to homozygous CMT1b mice, may be explained by a higher water content of the altered nerve, likely related to myelin envelop disruption.Regarding muscle, different from what expected, significant differences were not observed in T1 and T2* signals. At the microscopy evaluation, the thigh muscle appeared normal, without fat infiltration. This finding may be explained by a heterogeneous muscle involvement,

with a prevalent denervation atrophy of distal muscles of hindlimbs as expected in a length-dependent neuropathy.

Figure 1. Electron Microscopy of the myelin destructuration in MPZD61N/+ sciatic nerve and the matched WT

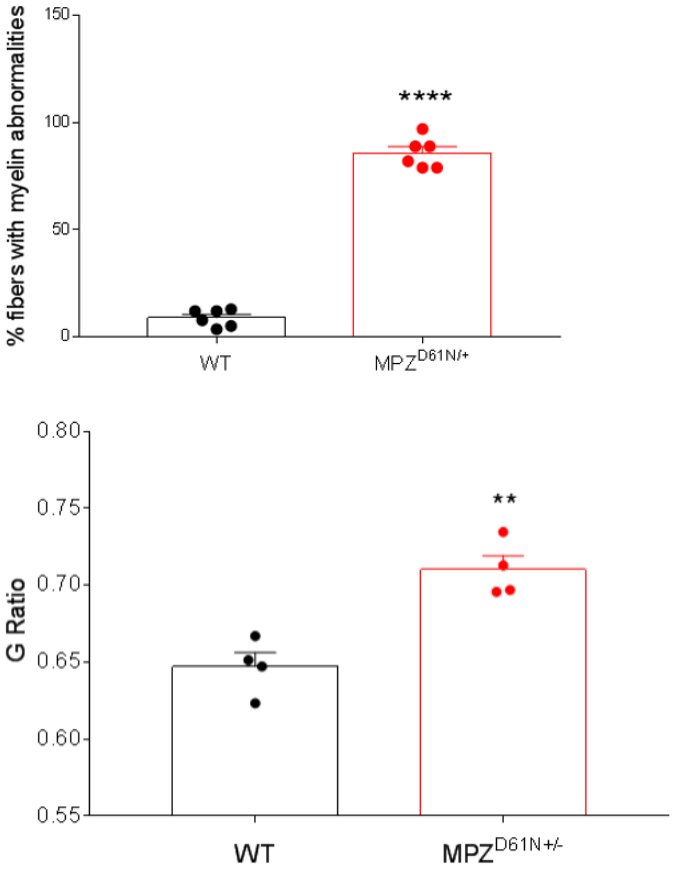

Figure 2- Distribution of myelin alteraion in Wt and MPZD61N/+ sciatic

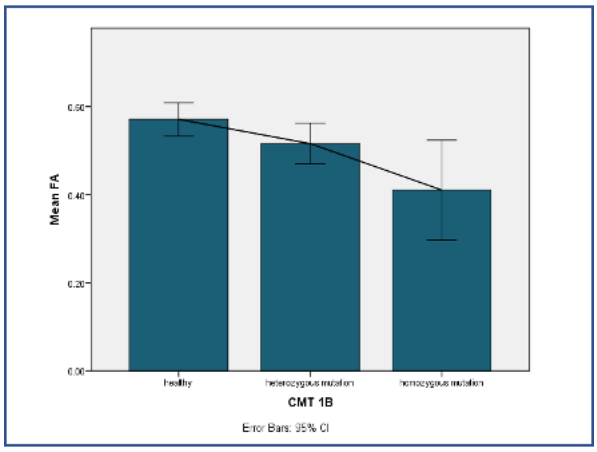

Graphic 1 . The decreasing values of sciatic nerve FA from WT to MPZD61N/+ is shown

A

B

Figure 2. Sagittal (A) and Axial (B) 3D T2 weighted with Inversion Recovery sequence of the sciatic nerve (yellow arrow) in *MPZD61N/+ mouse is shown.*

Conclusion

Even if this study represents a pilot MRI investigation of muscle and nerve in this severe form of CMT1B neuropathy, our results display that FA is sensitive enough to detect the nerve damage occurring in this CMT1B mouse model. Furthermore our results display that inflammatory cell may play a role in determining disease severity, and the higher is the inflammatory infiltrate, the lower is the FA value. Differently, further analysis and a more extensive muscle evaluation are needed to drive meaningful conclusion about the muscle alterations in this model and their detectability by MRI.

References

1. Veneri FA, Prada V, Mastrangelo R, Ferri C, Nobbio L, Passalacqua M, Milanesi M, Bianchi F, Del Carro U, Vallat JM, Duong P, Svaren J, Schenone A, Grandis M, D'Antonio M. A novel mouse model of CMT1B identifies hyperglycosylation as a new pathogenetic mechanism. Hum Mol Genet. 2022 Jul 31:ddac170.
2. Klein D, Groh J, Weishaupt A, Martini R. Endogenous antibodies contribute to macrophage-mediated demyelination in a mouse model for CMT1B. J Neuroinflammation. 2015 Mar 12;12:49
3. Kim HS, Yoon YC, Choi BO, Jin W, Cha JG, Kim JH. Diffusion tensor imaging of the sciatic nerve in Charcot-Marie-Tooth disease type I patients: a prospective case-control study. Eur Radiol. 2019 Jun;29(6):3241-3252.
4. Peng F, Xu H, Song Y, Xu K, Li S, Cai X, Guo Y, Gong L. Utilization of T1-Mapping for the pelvic and thigh muscles in Duchenne Muscular Dystrophy: a quantitative biomarker for

disease involvement and correlation with clinical assessments. BMC Musculoskelet Disord. 2022 Jul 16;23(1):681.
5. Marty B, Coppa B, Carlier PG. Monitoring skeletal muscle chronic fatty degenerations with fast T1-mapping. Eur Radiol. 2018 Nov;28(11):4662-4668. doi: 10.1007/s00330-018-5433-z. Epub 2018 Apr 30.

New Methodologies and Ultrasound Techniques for the Diagnosis and Clinical Management of Sarcopenia: development and application of a software for automated analysis of raw radiofrequency data

Background

Sarcopenia is a progressive disease of the striated muscles characterized by loss of skeletal muscle mass and function; it is strictly correlated with severe complications incl. falls, fractures, and, eventually, physical disability, leading to increased morbidity and mortality and poor quality of life. According to the revised European consensus of the European Working Group on Sarcopenia in Older People (EWGSOP), the diagnosis of sarcopenia requires the presence of low muscle strength and low muscle quantity or quality; when low physical performance occurs, sarcopenia is considered severe (1) . The detection of strength loss must be objectified by means of specific functional tests, such as the hand grip or the chair stand (2,3) . In regards to the non-invasive assessment of muscle quantity, magnetic resonance imaging (MRI) and computed tomography (CT) are referred to as the gold standards, but their high costs and limited availability restrict their use in clinical practice (4). The International Working Group on Sarcopenia (IWGS) and the Foundation for the National Institutes of Health (FNIH) agree in indicating Dual-energy x-ray absorptiometry (DEXA or DXA) as the most appropriate technique to quantify muscle depletion, whereas the EWGSOP suggests the use of Bioelectrical impedance analysis (BIA) depending on the clinical scenario, due to its affordability and portability(5). Nevertheless, these latter modalities have intrinsic weaknesses. BIA derives its estimate of muscle mass based on whole-body electrical conductivity, using a reference of DXA-measured lean mass based on older European populations for calibration purposes; therefore, its results are strongly influenced by age, ethnicity, and other related discrepancies between the reference population and patients. In addition, discrepancies can be found even

amongst different instrumentation companies, thus making it necessary to compare results with a specific standardization model5. On the other hand, DXA is strongly influenced by several factors, such as technical parameters, operator's experience and patient's hydration status, and can be inconsistent among different instrument companies (6-7). DXA instrumentation is not yet portable, and this comes as a significant disadvantage since primary care represents the first diagnostic contact for most of the sarcopenic elderly. Currently, most of health systems in western countries favor ageing-in-place over hospitalization in sanitary facilities. Finally, data provided by DXA and BIA only reflect muscle quantity without considering muscle quality and function, which are parameters that influence patient performance and prognosis. Due to its low cost, high availability and strong accuracy in measuring the muscle mass, ultrasound (US) appears a promising means to evaluate sarcopenic patients. It may also estimate the muscle quality by evaluating its echotexture (which increases in myosteatosis (9). The main US-based parameters assessed in the context of sarcopenia are: muscle thickness (MT), cross-sectional area (CSA), echo intensity (EI), pennation angle (PA), fascicle length (FL), and physiologic cross-sectional area (PCSA). Other parameters like vascularization and elastography are still under validation (10). Accordingly, a consensus protocol for US assessment of the muscle status in sarcopenic patients has been recently proposed (11) and it is conceivable that in the next few years there will be an increased use of this technique for diagnosing and following-up sarcopenia. Another interesting perspective offered by US is the possibility to perform a dynamic evaluation during muscle activation, thus providing information about muscle contraction. In this latter field, however, the use of US is still limited since the quality and interpretation of images is highly user dependent (12).

Objectives

The present study has four main objectives:
1: to identify new US-related parameters that may represent biomarkers of sarcopenia based on analysis of raw radiofrequency data provided by the US device.
2: to develop a software for an automated process of acquisition and interpretation of data without requiring subjective analysis by the examiner.
3: to provide prognostic stratification of sarcopenia based on the integration of clinical features and RF data to provide more objective information about muscle quantity, quality, and function.
4: to build the software in the machine for marketing purposes.

Methods

A multidisciplinary team composed of radiologists, neurologists, physiotherapists, engineers, and computer scientists will participate in the project. A biomedical company based in our city (Esaote spa: Via E.Melen, 16152, Genova, Italy) is involved with the aim of providing the facilities and expertise required to develop the system. The "raw" signals, which are commonly referred to as the radiofrequency (RF) data, are normally processed by the US machine to produce diagnostic images. However, RF data contains other information that is usually discarded during the process of creation of an US image. The analysis of RF data allows the extraction of additional information related to the tissue architecture and its modifications, with potential use in muscle evaluation. A highly reproducible and standardized scanning protocol for the acquisition of muscle US data will be defined, aiming at reducing interobserver variability. The US examination will be performed with a linear broadband high-frequency probes (frequency bands, 3-11MHz, 4-15MHz and 8-24MHz).
After developing and implementing the software for RF data analysis, the project will include three major sequential steps:

1. a series of patients undergoing CT at the Emergency Department of our University-Hospital for unrelated clinical purposes will be evaluated with US to recognize and grade sarcopenic abnormalities using a series of clinical tests and CT data as a reference.
2. a prospective observational cross-sectional study performed with US will be conducted using the developed software of analysis in two cohorts of patients. These cohorts will include age-stratified in-patients of our University-Hospital with suspected or already diagnosed sarcopenia and out-patients submitted to a rehabilitation program. A final analysis of data will be performed in order to develop a prognostic stratification system of the disease useful to improve the management protocol for the sarcopenic patient from the diagnosis to post-treatment.
3. a prospective longitudinal study performed with US using the developed software of analysis to measure the sensitivity of the system to detect changes of sarcopenia features occurring in those patients submitted to a specific rehabilitation program.

Relevance of the project

Sarcopenia is a high-prevalent and high-impacting disease with relevant economic implications: in the United States alone it has been reported that direct costs for hospitalization related to sarcopenia amount to 18.5 trillion dollars per year(13). It has been estimated that around 50 million people worldwide have sarcopenia (13) and with longer life expectancies of life the economic impact of sarcopenia is expected to continue to rise. In this scenario, the lack of a diagnostic tool providing an accurate and reliable evaluation of the status of the skeletal muscles represents a severe limitation for further improvements in terms of early diagnosis and treatment. A biomedical device allowing a standardized, rapid, and reliable evaluation of the morphologic features of the skeletal muscles may have a strong impact in sarcopenic patient care, as it could be employed in several contexts, such as hospital, rehabilitation centers or at home for self-monitoring. The technologic requirements for the development of such a proposed software for raw-data analysis built-in the device are not very demanding in terms of costs. Currently, portable US machines are widely used and several software for muscle recognition and segmentation have already been proposed in both clinical and research contexts. We believe that the project may be attractive for companies due to the potential marketability of this kind of application.

Project progress report

To date, a detailed protocol to collect Ultrasound and Radiofrequency images from the first cohort of patients have been developed (see step 1). All the patients presenting to the emergency department who needs a CT scan without contrast material of the chest and abdomen have been recruited. The Ultrasound examination wasn't executed on hemodynamically unstable or critical ill patients. The pectoralis major and the rectus abdominis have been identified as target muscle. A specific Ultrasound probe able to read the raw radiofrequency data, was developed, and a dedicated Ultrasound system was placed in the same room of CT scan machine. The probe was placed longitudinally respect to the muscle fibers. The images were saved exported in uncompressed DICOM format for external post-processing. The muscle density obtained by CT images in the same region of muscle Ultrasound sampling, was registered, the value expressed in Hounsfield Units were associated with the Ultrasound images in order to train the Artificial Intelligence system. According to our preliminary results, the AI supported software is able to identify the muscle density in a range of + or - 10 HU.

References

1) Cruz-Jentoft AJ, Bahat G, Bauer J, et al. Sarcopenia: revised European consensus on definition and diagnosis. Age Ageing 2019;48(1):16-31.
2) Sayer AA, Syddall H, Martin H, et al. The developmental origins of sarcopenia. J Nutr Health Aging 2008; 12:427–32.
3) Sayer AA, Syddall HE, Gilbody HJ et al. Does sarcopenia originate in early life? Findings from the Hertfordshire cohort study. J Gerontol A Biol Sci Med Sci 2004;59:M930–4.
4) Beaudart C, McCloskey E, Bruyère O. et al. Sarcopenia in daily practice: assessment and management. BMC Geriatr. 2016 Oct 5;16(1):170.
5) Guglielmi G, Ponti F, Agostini M, et al. The role of DXA in sarcopenia. Aging Clin Exp Res 2016;28(6):1047-1060.
6) Buckinx F, Landi F, Cesari M, et al. Pitfalls in the measurement of muscle mass: a need for a reference standard. J Cachexia Sarcopenia Muscle 2018; 9:269–78.
7) Kim KM, Jang HC, Lim S. Differences among skeletal muscle mass indices derived from height-, weight-, and body mass index adjusted models in assessing sarcopenia. Korean J Intern Med 2016; 31:643–50.
8) Strasser EM, Draskovits T, Praschak M, et al. Association between ultrasound measurements of muscle thickness, pennation angle, echogenicity and skeletal muscle strength in the elderly. Age 2013;35(6):2377-2388.
9) Mirón Mombiela R, Vucetic J, Rossi F, et al. Ultrasound Biomarkers for Sarcopenia: What Can We Tell So Far? Semin Musculoskelet Radiol. 2020 Apr;24(2):181-193.
10) Perkisas, S., Baudry, S., Bauer, J., et al. Application of ultrasound for muscle assessment in sarcopenia: towards standardized measurements. European geriatric medicine 2018, 9(6), 739-757.
11) Stringer HJ, Wilson D. The Role of Ultrasound as a Diagnostic Tool for Sarcopenia. J Frailty Aging. 2018;7(4):258-261.
12) Janssen I, Shepard DS, Katzmarzyk PT, et al. The healthcare costs of sarcopenia in the United States. J Am Geriatr Soc 2004;52(1):80-85.
13) Lenchik L, Boutin RD. Sarcopenia: beyond muscle atrophy and into the new frontiers of opportunistic imaging, precision medicine, and machine learning. Semin Musculoskelet Radiol 2018;22(03):307–322.